

Cutting shoe design for open caissons in sand: influence on vertical bearing capacity

Jack Templeman, Bryn Phillips and Brian Sheil

Jack O. Templeman

- MEng
- Department of Engineering Science, University of Oxford, Parks Road, Oxford OX1 3PJ, UK
- ORCID: 0000-0002-6991-4316

Bryn M. Phillips

- MEng
- Ward and Burke Construction Ltd, Unit N, Bourne End Business Park, Cores End Road, Bourne End, Bucks SL8 5AS, UK.

Brian B. Sheil

- BE PhD
- Royal Academy of Engineering Research Fellow, Department of Engineering Science, University of Oxford, Parks Road, Oxford OX1 3PJ, UK
- ORCID: 0000-0002-1462-1401

Corresponding author: Jack Templeman. Address: Department of Engineering Science, University of Oxford, Parks Road, Oxford OX1 3PJ, UK. Email: jack.templeman@eng.ox.ac.uk

Initial submission: 12 November 2020

Revised submission: 24 February 2021

Main text word count: 4929

Tables: 5

Figures: 17

Abstract

Open caisson shafts are a widely adopted solution for a range of geotechnical applications. An external 'cutting shoe' is a common construction feature used to reduce the soil frictional resistance acting on the caisson during sinking. This forms an annular void encircling the caisson which is filled with a support fluid to maintain excavation stability. The primary aim of this paper is to explore the influence of the cutting shoe geometry on the resulting vertical bearing resistance in sand. Finite element limit analysis is adopted for this purpose. Additional parameters considered in the modelling include the roughness of the cutting face and cutting shoe, and caisson radius and embedment depth. The results show that the influence of the cutting shoe is highly dependent on the caisson cutting face roughness and the soil friction angle, illustrated using detailed soil failure mechanisms. The roughness of the cutting shoe is also shown to cause a significant increase in the vertical soil reaction for large caisson embedment depths. By way of example, a recent UK case study, involving the construction of a 32 m diameter caisson, is used to highlight the potential influence of the cutting shoe on the bearing resistance during caisson sinking.

Keywords

Cofferdams & caissons, Excavation, Mathematical modelling

List of notations

B	caisson wall thickness
c	soil cohesion
f	vertical frictional stress on caisson wall, per unit length
h	external embedment depth
l	cutting shoe length ahead of cutting face
l_b	cutting shoe length behind cutting face
N	bearing capacity factor
R	caisson internal radius
t	cutting shoe thickness
v	vertical bearing stress on caisson wall base, per unit length
V	vertical bearing force on caisson wall base, per unit length
α_f	roughness factor of cutting face surface
α_s	roughness factor of cutting shoe surfaces
β	cutting face taper angle
γ'	soil unit weight
δ	interface friction angle
ϕ'	soil friction angle
ψ'	soil dilation angle

1. Introduction

Monolithic open caissons are a common method of constructing vertical shafts for a wide range of geotechnical applications including underground storage and attenuation tanks, launch and reception pits for tunnel construction, and deep foundations. Caisson construction uses concurrent casting of reinforced concrete walls and excavation of soil from within the structure, causing the caisson to 'sink' into the ground (see Figure 1). The sinking process requires careful control of the balance between the self-weight of the structure, W , and the upwards resistance generated from soil-structure interaction acting on the caisson walls (Sheil *et al.*, 2018). Rigorous predictions of these resistances, and their development during sinking, is therefore a key element of open caisson design and construction.

The design of the caisson wall incorporates important features to minimise soil penetration resistance as it sinks. A tapered cross-section or 'cutting face' is used at the base of the wall to reduce the vertical bearing capacity of the soil and mobilise soil failure towards the inside of the caisson for excavation (Royston *et al.*, 2016). To minimise frictional contact stresses, a 'cutting shoe' at the leading edge of the caisson wall creates an over-cut, which forms a void between the caisson wall and the surrounding soil as the structure sinks. This is typically referred to as the 'annulus' and is pumped with a support fluid, such as bentonite slurry, which acts to stabilize the excavation and lubricate the interface (Royston, 2018). Current practice often relies on the use of excessively thick caisson walls to provide sufficient self-weight to overcome the soil penetration resistance. Accurate estimation of the soil-structure contact stresses is critical in achieving efficient caisson design and reducing risk during construction.

Although the bearing capacity of the caisson wall critically affects the construction process, it has been under-explored in the literature. For large diameter caissons, the bearing capacity problem is analogous to an inclined strip footing, typically analysed by combining Terzaghi bearing capacity theory (Terzaghi, 1943) with published inclination and depth factors (e.g. Brinch Hansen, 1970; BSI, 2004). However, published studies explicitly exploring the open caisson problem are limited. Royston *et al.* (2016) and Chavda *et al.* (2020) describe small scale laboratory testing in sand aimed at exploring the penetration behaviour of a plane strain

footing section and a half-caisson model respectively. Various numerical techniques have also been applied including the slip line method (e.g. Solov'ev, 2008; Yan *et al.*, 2011), finite element analysis for frictional-cohesive soils (Chavda and Dodagoudar, 2018) and finite element limit analysis (FELA) for undrained soils (Royston *et al.*, 2020b). These investigations have largely focused on the role of the cutting face inclination angle and roughness, with the caisson wall geometry simplified by neglecting the presence of the cutting shoe and treating the entire external caisson-soil interface as either fully smooth (e.g. Royston *et al.*, 2020b) or partially rough (e.g. Chavda and Dodagoudar, 2018). Research on the effect of a cutting shoe therefore remains significantly less advanced.

This paper extends previous literature by exploring the role of the external cutting shoe in open caisson shaft construction, focusing on its impact on the geotechnical bearing resistance. The role of the cutting shoe in the sinking process is first discussed, outlining the practical considerations and issues faced during design and construction. A suite of FELA results is then presented, considering the influence of a cutting shoe on the vertical bearing resistance that develops on caissons during sinking in sands. Parameters investigated in the modelling include the cutting shoe geometry and roughness, soil friction angle, and caisson embedment and radius. By way of example, a recent UK case study, involving the construction of a 32 m internal diameter (ID) caisson (see Figure 1), is used to highlight the potential influence of the cutting shoe on the soil bearing resistance during caisson sinking.

2. Practical design considerations for an open caisson cutting shoe

Figure 2 provides a schematic illustration of an open caisson cross-section showing typical design features and soil-structure interaction resistances, including the bearing stresses at the base of the caisson (v) and the frictional resistance on the external surface of the caisson walls (f). The cutting shoe is a critical aspect of open caisson design and construction and serves three primary objectives:

- (a) Over-cut creation and support fluid delivery (Figure 3a): The over-cut is commonly formed by incorporating a steel cutting shoe around the leading edge of the caisson wall (e.g. Allenby *et al.*, 2009; Sheil *et al.*, 2018; Royston *et al.*, 2020a), such as in Figure

4a, or by casting a thicker wall section at the base (e.g. Ter-Galustov *et al.*, 1966; Nonveiller, 1987). The resulting annular gap between the external caisson surface and the surrounding soil is subsequently pumped with lubricant to provide hydraulic support to the surrounding soil. The lubricant-filled annulus minimises frictional resistance by preventing soil-structure contact or reducing the interface friction coefficient.

(b) Internal groundwater control (Figure 3b): the internal excavation level is often dewatered to enable excavation 'in the dry' by locating excavators at the dig level (as in Figure 1). This contrasts with excavation 'in the wet' involving a crane or excavator located at the external ground level and a clamshell bucket. Dewatering is typically passive, using hollow permeable tubes installed in the centre of the shaft. The cutting shoe is usually extended downwards, ahead of the apex of the cutting face. This increases the groundwater flow path from the exterior soil to the dewatered internal excavation level and potentially 'seals off' permeable sand lenses ahead of the excavation level thereby relaxing pumping requirements on site.

(c) Support fluid seepage/blow-out prevention (Figure 3c): by increasing the groundwater flow path, the cutting shoe also reduces the likelihood of support fluid loss through seepage from the annulus to the internal excavation level. For deep shafts, where the hydraulic pressure of the support fluid at the base of the annulus is high, the cutting shoe also helps to prevent a complete 'blow-out' of the annulus involving a rotational soil failure mechanism, as shown in Figure 3c.

Table 1 presents key caisson details for selected case histories published in the literature; these include the thickness of the caisson cutting shoe, governed by the resulting over-cut thickness requirements. For example, a larger over-cut thickness is often required in situations where significant ground swelling is expected during sinking (e.g. Nonveiller, 1987). In contrast, groundwater control and support fluid seepage/blow-out control the selection of an appropriate cutting shoe length, which typically extends up to 250 mm ahead of the cutting face, in the authors' experience.

These geometric requirements for the cutting shoe have important implications for the structural and geotechnical design of the caisson. A longer cutting shoe necessitates the inclusion of significant shear and flexural reinforcement within the caisson wall, leading to increased construction costs. Figure 4b shows an exemplar cutting shoe design and shear reinforcement (Royston, 2018; Royston *et al.*, 2020a). On the geotechnical side, the cutting shoe affects the vertical soil-structure interaction resistance by two competing mechanisms: (i) generation of the lubricated annulus leads to a significant reduction in the frictional soil resistance acting on the caisson wall; (ii) the cutting shoe effectively widens the base of the caisson and increases the depth of the soil failure mechanism, which both cause an increase in the vertical bearing capacity. It follows that for deep caissons, the former is likely to dominate (i.e. reduced frictional resistance) and vice versa for shallow embedments. However, there is currently no design guidance in the published literature or design codes.

3. Bearing capacity numerical study

3.1 Problem definition

Figure 5 outlines the problem definition and notation for this study. The caisson wall cross-section is described by the cutting face taper angle, β , caisson wall thickness, B , and internal radius, R . The cutting shoe is idealised as a rectangular appendage on the external surface of the caisson and is described by the cutting shoe thickness, t , extension ahead of the apex of the cutting face, l , and length behind the cutting face, l_b .

The caisson is considered embedded in homogeneous drained soil with friction angle ϕ' , cohesion $c' = 0$ and unit weight $\gamma' = 1 \text{ kN/m}^3$. The internal soil level is assumed coincident with the top of the cutting face, reflecting typical excavation of soil inside the caisson. The external embedment depth is denoted h and is defined relative to the internal soil surface. The roughness of the caisson and cutting shoe surfaces are defined by a roughness factor, α , such that the interface friction angle, δ , is given by $\tan \delta = \alpha \tan \phi'$ (Cassidy and Houlsby, 2002), where values of α of 0 and 1 denote a fully smooth and fully rough interface respectively.

The soil exerts a vertical bearing force per unit length, V , on the caisson wall section. This is expressed as a dimensionless bearing capacity factor, N' , defined as:

$$N' = 2 \frac{V}{\gamma'(B + t)^2} \quad (1)$$

where $B + t$ is the overall width at the base of the caisson wall section (see Figure 5).

3.2 Details of numerical modelling

The numerical analyses described in this paper were performed using the FELA software package Optum G2 (Optum G2, 2020). The soil was modelled as a 2D domain of rigid-plastic material obeying the Mohr-Coulomb failure criterion with an associated flow rule (soil dilation angle, $\psi' = \phi'$). In each analysis, the domain was defined to be sufficiently large to avoid any boundary/edge effects on the soil failure mechanism. Boundary conditions were applied to restrict lateral displacement of the vertical sides of the domain and to restrict displacement in all directions on the domain base. The caisson wall section and cutting shoe were modelled as a single rigid body with the interface roughness factor of the cutting face and shoe surfaces defined by α_f and α_s respectively (see Figure 5). In this study the lubricated annulus is assumed to be fully supported, such that no lateral displacement of the external soil surface is allowed and no frictional stresses develop above the cutting shoe.

The following stages of analysis were adopted in the modelling:

- I. Wished-in-place installation of the caisson wall section to an embedment depth h in a soil domain with friction angle ϕ' . Movement of the footing is fully restrained during this calculation step.
- II. Application of a downward load multiplier to the caisson wall section until failure is achieved. During this step only vertical displacement of the caisson is allowed (lateral displacement and rotation restrained).

In each analysis strict lower- (LB) and upper-bound (UB) plasticity solutions were computed, bracketing the exact collapse load. The error between the bounds can be defined by:

$$error = \pm \frac{UB - LB}{(UB + LB)} \quad (2)$$

The LB analyses used triangular elements with a linear variation in stresses between corner nodes such that yield conditions are enforced at the three corner nodes. The UB analyses used triangular elements with quadratic interpolation of displacements and linear interpolation of stresses within each element. Each model was initially uniformly discretised with 1,000 elements, before iterating through eight rounds of adaptive mesh refinement based on the distribution of plastic shear dissipation. After several remeshing iterations, the concentration of elements in the mesh reflects the characteristics of the soil failure mechanisms. The maximum number of elements at the end of the analysis was varied depending on the size of the model, to allow a sufficiently small error to be achieved. In all analyses the error was less than $\pm 3\%$ and the final collapse loads were obtained by averaging the LB and UB collapse multipliers at the end of the analysis.

3.3 Overview of numerical study

The numerical analyses in this study consider a caisson footing with a taper angle $\beta = 45^\circ$, reflecting common design in industry (Fischer *et al.*, 2004; Royston *et al.*, 2016). The influence of a smooth cutting shoe ($\alpha_s = 0$) on the vertical bearing resistance of a shallow inclined footing is investigated first. In these analyses, the caisson is embedded to $h/B = 0$ (i.e. the soil surface is level with the top of the cutting face on both sides of the footing). The problem is initially treated as plane strain ($B/R = 0$), which is applicable to large-diameter caissons. The influence of dimensionless cutting shoe thickness, t/B , and length, l/B , are considered in turn, using a parameter space covering the cutting shoe geometries documented in the literature. A limited number of additional FELA analyses are subsequently undertaken to investigate the influence of a cutting shoe at deeper embedment depths and for different caisson radii. A 'typical' cutting shoe defined by $t/B = 0.07$ and $l/B = l_b/B = 0.25$ is used in those analyses, derived from the authors' experience.

4 Numerical results

4.1 Influence of cutting shoe thickness

The influence of the cutting shoe thickness, t , on the vertical bearing capacity of the caisson is explored using the parameter set presented in Table 2; in these initial analyses the cutting shoe is assumed to have zero length ($t/B = 0$). The FELA-predicted capacity for the no cutting shoe case, $N'_{t=0}$, is first plotted in Figure 6, considering both a smooth ($\alpha_f = 0$) and rough ($\alpha_f = 1$) cutting face and for values of ϕ' between 15° and 45° . It can be seen that α_f has a significant influence on the footing bearing capacity.

The influence of a cutting shoe inclusion with a dimensionless thickness t/B on the vertical bearing capacity is presented in Figure 7; these results are plotted as the numerically-predicted N' values normalised by the corresponding $N'_{t=0}$ values from Figure 6. Considering first the results for $\alpha_f = 0$, an increase in t/B causes a significant increase in capacity relative to the 'no shoe' case. This is particularly the case for high- ϕ' soil due to significant changes in the soil failure mechanism. Figure 8 shows failure mechanisms corresponding to $t/B = 0$ and $t/B = 0.1$ for the extremum friction angles ($\phi' = 20^\circ$ and 45°). It can be seen that the failure mechanism is confined entirely to the internal side, for all values of ϕ' , when no cutting shoe is used (e.g. Figures 8a,c). For low ϕ' , the cutting shoe causes a larger and deeper mechanism to form but the mechanism remains on the internal side only (see Figure 8b). In contrast, for high ϕ' , the cutting shoe causes the failure mechanism to develop on both the internal and external sides (Figure 8d), hence resulting in a greater increase in $N'/N'_{t=0}$ compared to low ϕ' . The detail in Figures 8b,d show that the change in failure mechanism is primarily due to the formation of a rigid 'false head' directly beneath the cutting shoe, which increases in size with t/B . This causes both an increase in the confining stress on the failure surfaces and an increase in their length, as the failure mechanism forms from the tip of the false head.

For $\alpha_f = 1$ in Figure 7, the presence of a cutting shoe causes a decrease in $N'/N'_{t=0}$. For low ϕ' the mechanism only forms on the internal side and a small false head again forms beneath the cutting shoe (see Figures 9a,c). For high ϕ' , the failure mechanism forms a much larger rigid wedge along the taper face, both with and without a cutting shoe, as shown in Figures 9b,d. This effectively steepens the inclination of the cutting face (i.e. the apparent β angle decreases), as the failure mechanism extends from the tip of the wedge. A smaller secondary false head

forms beneath the cutting shoe for $t/B > 0$, with an additional shear band in the mechanism on the external side (see Figure 9d). This has a minor influence on the bearing capacity as the majority of the failure mechanism remains unchanged, including the larger wedge of soil trapped at the cutting face.

4.2 Influence of cutting shoe length

The influence of the dimensionless cutting shoe extension length l/B on the vertical bearing capacity is considered in Figures 10 and 11 for $\alpha_f = 0$ and $\alpha_f = 1$ respectively. The numerically predicted capacities are again normalised by the no cutting shoe values, $N_{t=0}$. In all cases, extending the cutting shoe ahead of the apex of the cutting face increases the normalised bearing resistance. This is to be expected as the cutting shoe extends deeper into the soil with increased l , resulting in increased confining stresses on the soil shear planes and a larger failure mechanism size. Interestingly, normalising the bearing capacity in this way achieves a negligible influence of t/B on the resulting trends in these figures, particularly for soils with low friction angles. Similarly, Figure 10 and Figure 11 also do not show any clear trend with respect to ϕ' . This can be attributed to complex changes that occur in the failure mechanisms as the cutting shoe extends ahead of the taper face for different ϕ' .

Examples of the failure mechanisms at extremum friction angles are given in Figure 12 and Figure 13 for smooth and rough cutting face respectively, where values of $t/B = 0.1$ and $l/B = 0.4$ are adopted for illustrative purposes. For $\alpha_f = 0$ and $\phi' = 20^\circ$, Figure 12a shows that an extension of the cutting shoe ahead of the taper face now causes the soil failure mechanism to extend to the external side which was not present for the $l/B = 0$ case when compared to Figure 8b. An increase in ϕ' to 45° leads to a deeper 'external mechanism' for increased l , as shown in Figure 12b. In all cases, the internal mechanism forms at the apex of the cutting face and is relatively unaffected by any extension of the cutting shoe when the cutting face is smooth. Conversely for $\alpha_f = 1$ and $\phi' = 20^\circ$, a wedge of soil becomes 'trapped' behind the cutting shoe (Figure 13a) which is not present when $l/B = 0$ (Figure 9b). This again causes an effective steepening of the footing resulting in no external mechanism developing and an enlarging of the

internal mechanism. Figure 13b shows that for $\phi' = 45^\circ$, the rigid soil wedge at the cutting face increases in size with increasing l , forming from the tip of the cutting shoe.

The analyses presented in Sections 4.1 and 4.2 consider very shallow penetration ($h/B = 0$) and also assume a fully smooth cutting shoe ($\alpha_s = 0$) to isolate friction effects from the bearing resistance contribution. Including the effects of cutting shoe friction would therefore lead to higher overall bearing resistances.

4.3 Influence of embedment depth and cutting shoe roughness

Figure 14 plots the predicted influence of the dimensionless external embedment depth, h/B , on the vertical bearing capacity, using the parameters presented in Table 3. These analyses consider both a smooth and rough cutting face for a typical sized cutting shoe used in practice ($t/B = 0.07$ and $l/B = l_b/B = 0.25$). The results are normalised by the corresponding $N'_{t=0}$ value at h/B . The results reveal the occurrence of a 'critical embedment depth' beyond which a further increase in h/B has a negligible effect on N' . For low values of h/B , the bearing capacity increases with depth due to the extension of the failure mechanism on the external side of the footing. However, once the critical embedment depth has been reached, the failure mechanism becomes confined to the internal side only, resulting in a negligible increase in bearing capacity with further increases in h/B . The addition of a cutting shoe significantly influences the relationship between h/B and N' which also appear highly dependent on the roughness of the cutting shoe (see Figure 14).

In all cases, a smooth cutting shoe ($\alpha_s = 0$) appears to cause a minor increase in bearing capacity and an insignificant alteration to the role of h/B . This is because the failure mechanism remains largely unchanged and is confined to the internal side at a very similar h/B . Figure 14d shows that in the case of $\alpha_f = 1$ and for high ϕ' , the use of a smooth cutting shoe actually reduces the bearing capacity factor. This is again due to the effective steepening of the footing causing the failure mechanism to be confined to the internal side at lower embedment depths compared to when no cutting shoe is used.

Increasing the roughness of the cutting shoe results in significantly larger bearing capacities and greater dependence on embedment depth, particularly for high- ϕ' soils. For example, a rough cutting shoe in $\phi' = 20^\circ$ soil causes an increase in bearing capacity by a factor of ~ 1.6 and ~ 1.4 (relative to the $h/B = 0$ case) for $\alpha_f = 0$ and $\alpha_f = 1$ respectively, eventually reaching a critical embedment depth of $h/B \approx 5$ (see Figures 14a and 14c). In contrast, the critical embedment depth for $\phi' = 45^\circ$ varies between $h/B = 50$ and 70 , as shown in Figures 14b and 14d. Salient failure mechanisms for the $\alpha_f = 1$ and $\alpha_s = 1$ case are shown in Figure 15. The cutting shoe causes the external failure mechanism to remain for much deeper embedment depths (Figure 15a-c) before eventually transitioning to the internal side only (Figure 15d). This leads to a significant increase in the bearing capacity, particularly for a rough cutting shoe; in this case the capacity increases by a factor of 14 and 5, relative to the $h/B = 0$ case, for a $\alpha_f = 0$ and $\alpha_f = 1$ respectively. The detail in Figure 15d shows that the rough external cutting shoe surface (of length $l_b + l$) causes a wedge of soil on the outside of the caisson to be dragged downwards. The external wedge, in turn, causes a larger and deeper failure mechanism that encompasses the full extent of the cutting shoe.

4.4 Influence of caisson radius

Figure 16 plots the predicted vertical bearing capacity as a function of the reciprocal of the dimensionless caisson radius (B/R) using the parameters shown in Table 4. The results are normalised by the corresponding plane strain value ($N'_{R=\infty}$). In all cases, an increase in B/R (smaller caisson radii) causes an increase in $N'/N'_{R=\infty}$ due to an increase in radial stress and therefore confining stress. The results for both $\alpha_f = 0$ (Figure 16a) and $\alpha_f = 1$ (Figure 16b) show that for high- ϕ' soil there is a significant dependency of N' on B/R , regardless of the cutting shoe design. The addition of a smooth cutting shoe ($\alpha_s = 0$) causes an increase in the bearing resistance with B/R for all cases considered here. A similar, but greater increase, is also observed for a rough cutting shoe ($\alpha_s = 1$) and low- ϕ' soil. In these cases, the failure mechanism is only present on the internal side of the footing. For $\phi' = 45^\circ$ and $\alpha_f = 1$, the addition of a cutting shoe with $\alpha_s = 1$ causes the relationship between B/R and $N'/N'_{R=\infty}$ to become non-linear. This is because of the presence of an external failure mechanism, which is present throughout the range of B/R considered in Figure 16.

5. Case study

5.1 Project details

To illustrate practical implications of the present numerical results, a recent case study is considered involving the construction of a 32m ID open caisson in dense sand by Ward & Burke Construction Ltd in Blackpool, UK (see Figure 1). Key caisson and soil parameters documented for this caisson are presented in Table 5 (Royston, 2018). For the purposes of this study, the bearing capacity was considered over the embedment range $h = 0 - 12.5$ m and the cutting face has been assumed fully rough ($\alpha_r = 1$). Additional details on the project are presented in Royston (2018) and Royston *et al.* (2020a). The cutting shoe thickness used during the installation was 75 mm and the shoe has been assumed to have a 250 mm length behind the apex of the taper.

5.2 Results and implications for design

Figure 17 plots the FELA-predicted vertical bearing capacity for the Blackpool caisson considering several different cutting shoe designs. At the final embedment depth of $h = 12.5$ m, it can be seen that the choice of the cutting shoe has a remarkable influence on the resulting bearing capacity. For the case of a smooth cutting shoe, there is only a minor increase in the predicted bearing resistance relative to the no cutting shoe case and the critical embedment depth is reached at $h \approx 2$ m. The dependence of the bearing capacity on the length of the cutting shoe also appears relatively insignificant, with the increased length of the shoe actually reducing the bearing resistance slightly. In contrast, for non-smooth cutting shoes, a significant increase in the bearing capacity with depth is observed and the cutting shoe extension length begins to have an appreciable influence. This situation is undesirable in practice as it may then be necessary to underream the caisson cutting face to sink the caisson which is to have an adverse effect on the construction schedule. The frictional stresses that develop on a cutting shoe in practice may be high given the relatively rough steel-soil interface and possible large horizontal pressures exerted on the shoe. This highlights the importance of achieving a smooth finish with the fabrication of the cutting shoe, particularly where a long extension is required for groundwater/lubricant control etc.

Furthermore, for $\alpha_s = 0.5$ and 1 the results show that achieving the critical embedment depth is unlikely for this project and therefore deeper embedments are expected to increase the bearing capacity even further. This further increases the risk of deep caisson shafts becoming wedged in dense sands (i.e. failure to sink to formation depth). The significant bearing resistances generated due to the addition of the cutting shoe also have important implications for the structural design of the shoe for buckling prevention and to ensure the integrity of the shoe-wall connection.

6. Limitations of modelling

The analyses completed in this paper have important limitations which should be carefully considered when taking these results into account for design in practice. A simple rectangular cross-section was adopted for the cutting shoe in the modelling and more complex geometries (with bevelled edges for example) are likely to have a non-negligible influence. Similarly, the present treatment of the annulus as a perfectly smooth rigid boundary tacitly assumes that the annulus remains open during sinking. However, failure of the annulus is possible in sands and this may lead to even more complex failure mechanisms. The 'wished-in-place' installation process also neglects the influence of any deformation-induced changes to the soil on the vertical capacity, such as geometry changes (e.g. soil heave) or alteration of the soil material properties. Large displacements may also have considerable impact on the soil-structure interface roughness as the caisson sinks, with changes in the interface friction angle and possible grain crushing occurring (Ho *et al.*, 2009). To overcome this simplification, a more sophisticated form of large-deformation numerical analysis would be required.

Another important limitation of this study is the simplified constitutive model used. The shear resistance, stiffness and dilatancy of sand has strong dependence on its density, confining stress and the shear strain it is subject to. The assumption of associated flow with perfectly plastic Mohr-Coulomb failure is expected to over-estimate the caisson bearing capacity in practice, particularly in soils with high friction angles (e.g. Loukidis and Salgado, 2009). The primary risk in caisson sinking is underestimating the resistance from the soil and the structure

having insufficient self-weight to continue sinking. The resulting bias of the present predictions are therefore on the safe side for this problem such that these results may be transferred to practice with confidence.

Finally, the soil dewatering process, and associated groundwater flow, is likely to reduce the effective stresses in the soil and, in turn, the vertical resistance of the soil, particularly towards the caisson interior. This may further encourage the failure mechanisms to propagate internally. It is also possible that the dewatering process could cause dissipation of lubricant from the annulus into the surrounding soil, which could further alter the soil and soil-structure interface properties. This study assumes that an adequate assessment of this process has been completed.

7. Conclusions

This paper has described a numerical study of the role of a cutting shoe on the drained bearing capacity of an open caisson cutting face. Finite element limit analysis was used to explore the role of the caisson cutting shoe geometry and roughness on the vertical soil reaction. Additional parameters considered in the modelling included the roughness of the cutting face, and the caisson radius and embedment depth.

The parametric study revealed that the inclusion of a cutting shoe has a significant influence on the vertical soil reaction during sinking and is highly dependent on the roughness of the cutting face, the friction angle of the soil, the caisson embedment depth and, to a lesser extent, the caisson radius. The inclusion of a typical sized cutting shoe used in industry caused substantial increases in bearing capacity for deep caisson embedments in high- ϕ' soil. In particular, the influence of cutting shoe roughness was shown to be considerable. This highlights the additional risks associated with the construction of deep open caisson shafts in dense sands.

Interestingly, the presence of a cutting shoe causes a greater increase in the bearing capacity when the cutting face is smooth. This was shown to be due to the formation of a rigid false head at the tip of the shoe which altered the soil failure mechanism. In addition, it was shown that

when the cutting shoe is smooth, the most important geometric factor is the shoe thickness. In contrast, if the shoe is rough, then the shoe length tends to dominate the bearing capacity.

Acknowledgements

The authors gratefully acknowledge the support of Ward & Burke Construction Ltd during this research. This work was supported by the Royal Academy of Engineering under the Research Fellowship Scheme and the Engineering and Physical Sciences Research Council (grant no. EP/T006900/1).

References

- Abdrabbo, F and Gaaver, K (2012) Challenges and Uncertainties Relating to Open Caissons. *J. Deep Found. Inst.* **6(1)**: 21–32.
- Allenby, D, Waley, G and Kilburn, D (2009) Examples of open caisson sinking in Scotland. *Proceedings of the Institution of Civil Engineers - Geotechnical Engineering* **162(1)**: 59–70, <https://doi.org/10.1680/geng.2009.162.1.59>.
- Brinch Hansen, J (1970) *A revised and extended formula for bearing capacity*. Bulletin No. 28. The Danish Geotechnical Institute.
- BSI (2004) *Eurocode 7: Geotechnical design - Part 1: General rules (BS EN 1997-1)*. London: British Standards Institution.
- Cassidy, MJ and Houlsby, GT (2002) Vertical bearing capacity factors for conical footings on sand. *Géotechnique* **52(9)**: 687–692, <https://doi.org/10.1680/geot.2002.52.9.687>.
- Chavda, JT and Dodagoudar, GR (2018) Finite element modelling of extent of failure zone in c - ϕ soil at the cutting edge of open caisson. in *Numerical Methods in Geotechnical Engineering IX. 9th European Conference on Numerical Methods in Geotechnical Engineering (NUMGE 2018)*, Porto, Portugal: Taylor & Francis, 999–1007.
- Chavda, JT, Mishra, S and Dodagoudar, GR (2020) Experimental evaluation of ultimate bearing capacity of the cutting edge of open caisson. *International Journal of Physical Modelling in Geotechnics* **20(5)**: 281–294, <https://doi.org/10.1680/jphmg.18.00052>.
- Fischer, GR, Gerszewski, WL, Barchok, FJ and Yavarow, MK (2004) Deep Caisson Sinking in Soft Soils, Grand Forks, North Dakota. in *Proceedings of the 5th International Conference on*

Case Histories in Geotechnical Engineering. International Conference on Case Histories in Geotechnical Engineering, New York, NY, USA: Paper 1.67, Available at: <https://scholarsmine.mst.edu/icchge/5icchge/session01/42>.

Ho, YK, Jardine, RJ and Anh-Minh, N (2011) Large displacement interface shear between steel and granular media. *Géotechnique* **61**(3): 221–234, <https://doi.org/10.1680/geot.8.P.086>.

Loukidis, D and Salgado, R (2009) Bearing capacity of strip and circular footings in sand using finite elements. *Computers and Geotechnics* **36**: 871–879, <https://doi.org/10.1016/j.compgeo.2009.01.012>.

Nonveiller, E (1987) Open Caissons for Deep Foundations. *Journal of Geotechnical Engineering* **113**(5): 424–439, [https://doi.org/10.1061/\(ASCE\)0733-9410\(1987\)113:5\(424\)](https://doi.org/10.1061/(ASCE)0733-9410(1987)113:5(424)).

Optum G2 (2020). Optum CE.

Royston, R (2018) *Investigation of Soil-Structure Interaction for Large Diameter Caissons*. DPhil Thesis. University of Oxford.

Royston, R, Phillips, BM, Sheil, BB and Byrne, BW (2016) Bearing capacity beneath tapered blades of open dug caissons in sand. in *Proceedings of Civil Engineering Research in Ireland 2016. Civil Engineering Research in Ireland 2016*, Galway, Ireland: Civil Engineering Research Association of Ireland 473–478.

Royston, R, Sheil, BB and Byrne, BW (2020a) Monitoring the construction of a large-diameter caisson in sand. *Proceedings of the Institution of Civil Engineers - Geotechnical Engineering*, <https://doi.org/10.1680/jgeen.19.00266>.

Royston, R, Sheil, BB and Byrne, BW (2020b) Undrained bearing capacity of the cutting face of large-diameter caissons. *Géotechnique*. DOI: 10.1680/jgeot.20.P.210.

Sheil, BB, Royston, R and Byrne, BW (2018) Real-Time Monitoring of Large-Diameter Caissons. in *Proceedings of China-Europe Conference on Geotechnical Engineering, SSGG. China-Europe Conference on Geotechnical Engineering 2018*, Vienna, Austria: Springer 725–729, https://doi.org/10.1007/978-3-319-97112-4_162.

Solov'ev, NB (2008) Use of limiting-equilibrium theory to determine the bearing capacity of soil beneath the blades of caissons. *Soil Mechanics and Foundation Engineering* **45**(2): 39–45.

441 Ter-Galustov, SA, Ponomarenko, AI, Opershtein, VL and Ivanov, VD (1966) Experience in
442 sinking an open caisson in a thixotropic lining. *Soil Mechanics and Foundation Engineering* **3**
443 128–131, <https://doi.org/10.1007/BF01703486>.
444 Terzaghi, K (1943) *Theoretical Soil Mechanics*. New York: John Wiley & Sons, Inc.,
445 <http://dx.doi.org/10.1002/9780470172766>.
446 Yan, FY, Guo, YC and Liu, SQ (2011) The Bearing Capacity Analyses of Soil beneath the Blade
447 of Circular Caisson. *Advanced Materials Research* **250–253** 1794–1797.
448

Tables

Table 1 Key parameters from selected open caissons in the published literature.

Reference	Internal radius, R (m)	Total caisson depth (m)	Wall width, B (m)	Cutting face inclination, β (°)	Cutting shoe thickness, t (m)	Ground conditions	Over-cut formation method	Annulus Lubrication
Ter-Galustov <i>et al.</i> (1966)	7.7	14.1	0.3	Not given	0.1	Dense dry loams	Thicker concrete wall section	Clay-based mud
Nonveiller (1987)	13.5	60	1.5	34.1	0.2	Stiff clay	Thicker concrete wall section with steel cutting edge	Stabilised bentonite slurry
Fischer <i>et al.</i> (2004)	9.15	22.86	0.91	45	0.15	Clays with some silt/sands	Thicker concrete wall section	Bentonite
Abdrabbo and Gaaver (2012)	10	33.31	1.6	40.4	0.1	Dense sand with sandstone, overlaying sandy silt and silty clay	Thicker-concrete wall section	Not given
Royston (2018)	5.5	20	1	60	0.07	Soft clay overlaying mudstone	Steel cutting shoe	Polymer
Royston (2018)	12.5	15	1	45	Not given	Soft peat, overlaying medium dense sand, founding on stiff clay	Steel cutting shoe	Bentonite and polymer
Royston (2018); Sheil <i>et al.</i> (2018); Royston <i>et al.</i> (2020a)	16	20	1.25	45	0.075	Dense sand overlaying stiff clay	Steel cutting shoe	Bentonite and polymer

Table 2 Parameters adopted in the FELA analyses of the influence of cutting shoe geometry on the vertical bearing capacity of the caisson.

Parameter	Values
B/R	0
h/B	0
ϕ'	15, 20, 25, 30, 35, 40, 45°
t/B	0, 0.05, 0.1, 0.15, 0.2
l/B	0, 0.1, 0.2, 0.3, 0.4
α_f	0, 1
α_s	0

Table 3 Parameters adopted in the FELA analyses to explore the influence of a typical sized cutting shoe of varying roughness on caisson vertical bearing capacity for a range of embedment depths.

Parameter	Values
B/R	0
h/B	0, 2, 5, 10, 15, 20, 30, 50, 70, 90
ϕ'	20, 45°
t/B	0.07
l/B	0.25
l_b	0.25
α_i	0, 1
α_s	0, 0.25, 0.5, 1

Table 4 Parameters adopted in the FELA analyses to explore the influence of a typical sized cutting shoe of varying roughness on caisson vertical bearing capacity for a range of caisson internal radii.

Parameter	Values
B/R	0, 0.1, 0.2, 0.286, 0.5
h/B	30
ϕ'	20, 45°
t/B	0.07
l/B	0.25
l_b	0.25
α_i	0, 1
α_s	0, 1

Table 5 Parameters adopted in the FELA analyses of the Blackpool case study

Parameter	Value
R	16 m
B	1.25 m
ϕ'	40°
γ'	20 kN/m ³
t	0.075 m
l	0, 0.25 m
l_b	0.25 m
α_f	1.0
α_s	0, 0.5, 1.0

Figure captions



Figure 1 Construction of a 32 m ID caisson shaft by Ward & Burke Construction Ltd in Blackpool, UK.

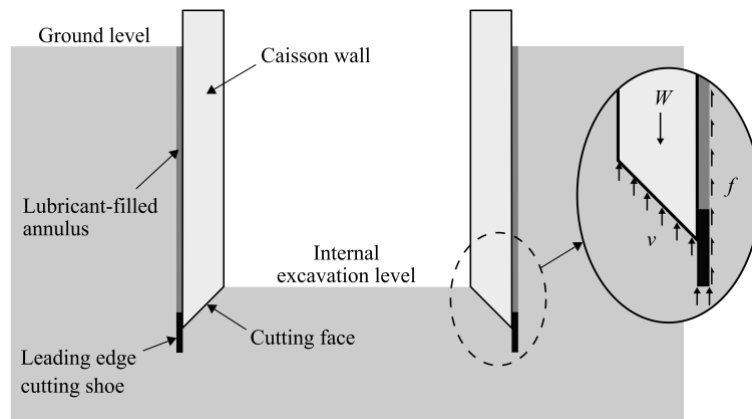


Figure 2 Schematic illustration of a section through an open caisson shaft, showing typical construction features and a detail of the forces on the caisson wall during sinking.

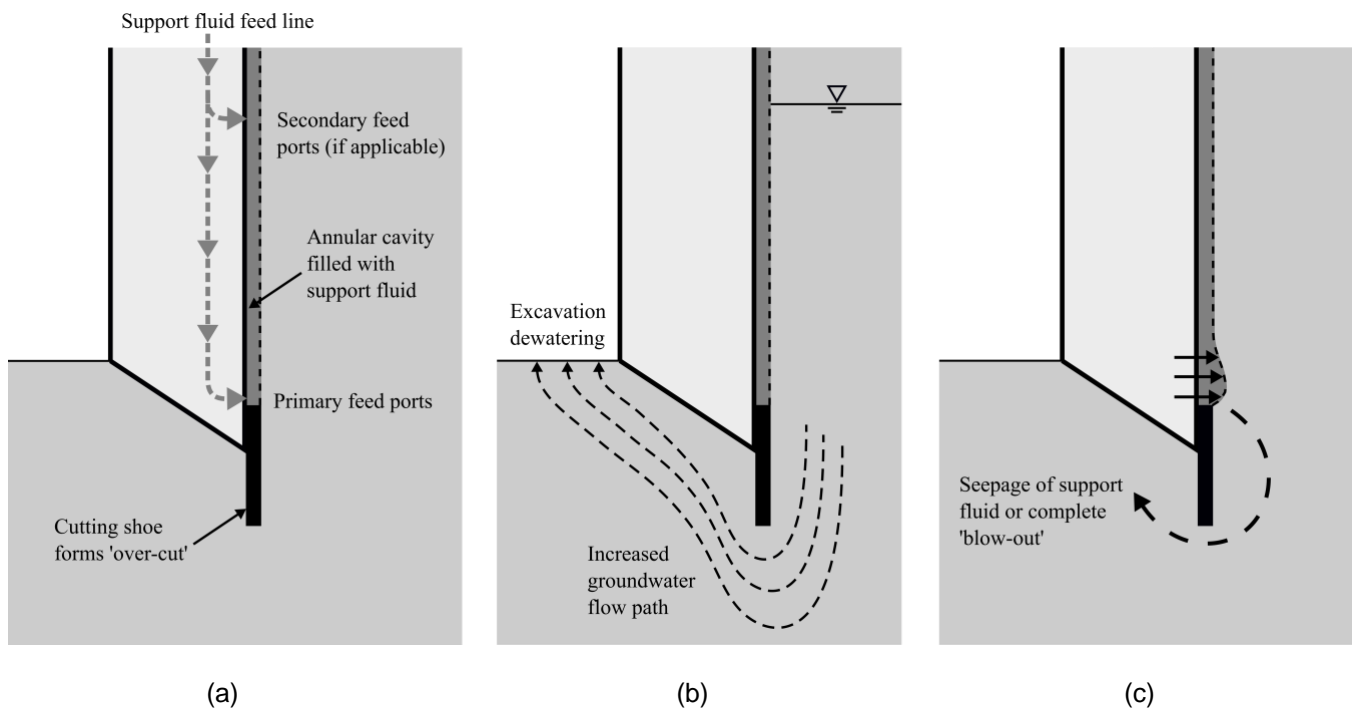
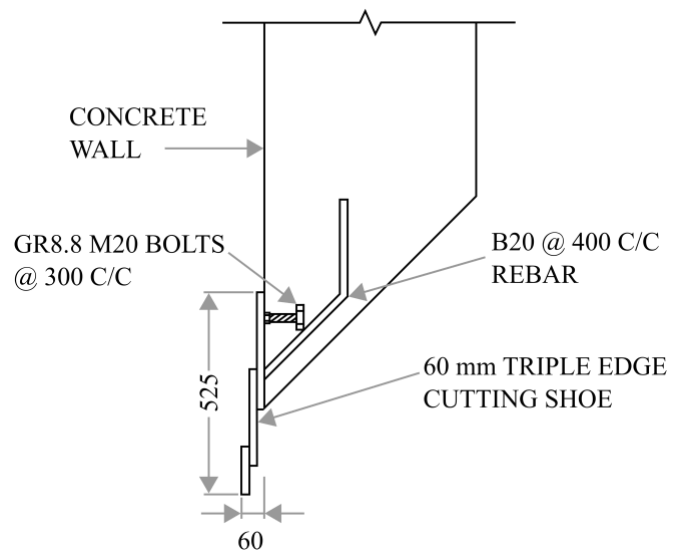


Figure 3 Schematic illustration of the main roles of the cutting shoe in open caisson construction: (a) over-cut creation and support fluid delivery, (b) groundwater control and (c) support fluid seepage/blow-out prevention.



(a)



(b)

Figure 4 Examples of a typical steel caisson cutting shoe: (a) photo of an assembled cutting shoe with a visualisation of the concrete caisson wall and (b) section drawing showing details of cutting shoe geometry and reinforcement.

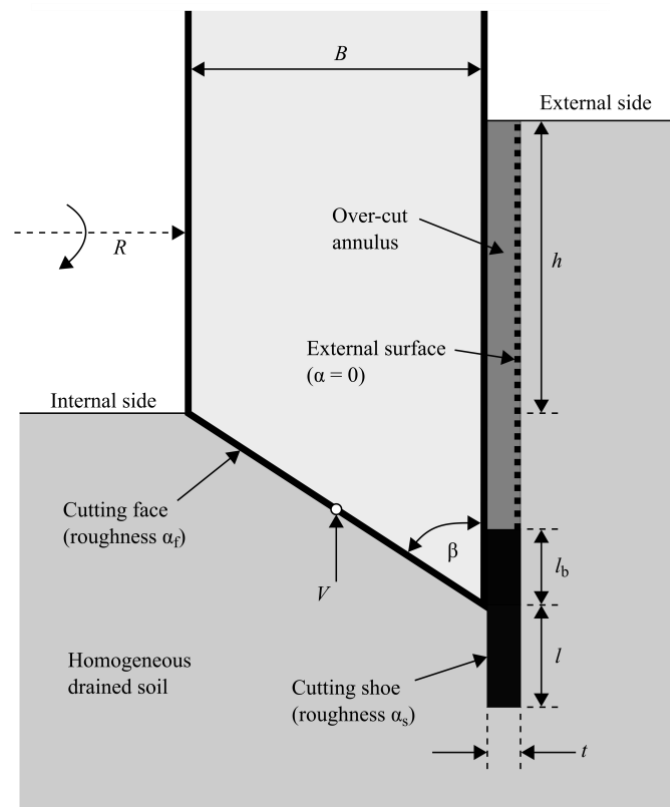


Figure 5 Problem definition for the bearing capacity numerical study, including geometric parameters and interface roughness factors.

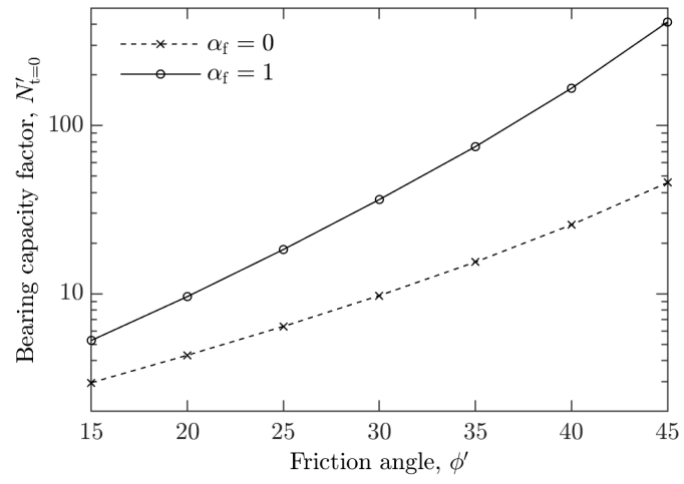


Figure 6 Numerical predictions of the vertical bearing capacity for a $\beta = 45^\circ$ footing with no cutting shoe ($t/B = 0$ and $l/B = 0$) and both a smooth ($\alpha_f = 0$) and rough ($\alpha_f = 1$) cutting face; $B/R = 0$ (plane strain), $h/B = 0$.

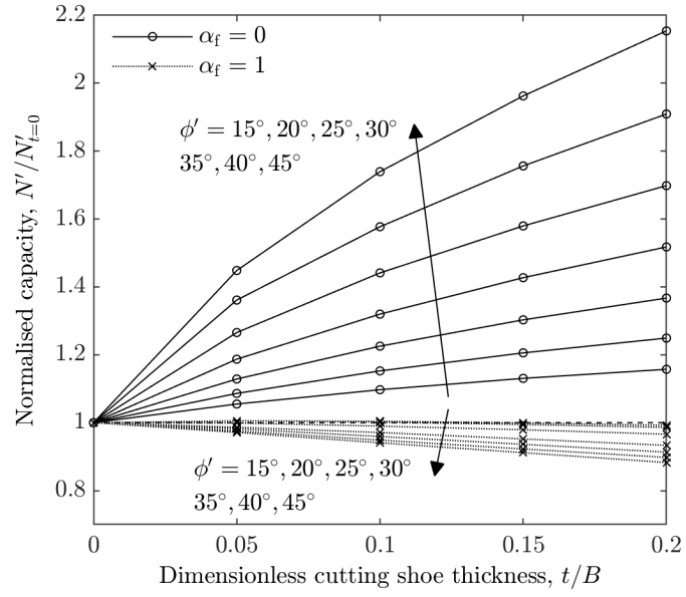


Figure 7 Numerical predictions of the influence of a cutting shoe with thickness t/B on the vertical bearing capacity of a $\beta = 45^\circ$ footing considering both a smooth ($\alpha_f = 0$) and rough ($\alpha_f = 1$) cutting face. Results are normalised by the corresponding values with no cutting shoe ($N'_{t=0}$); $B/R = 0$ (plane strain), $h/B = 0$, $\alpha_s = 0$, $l/B = 0$.

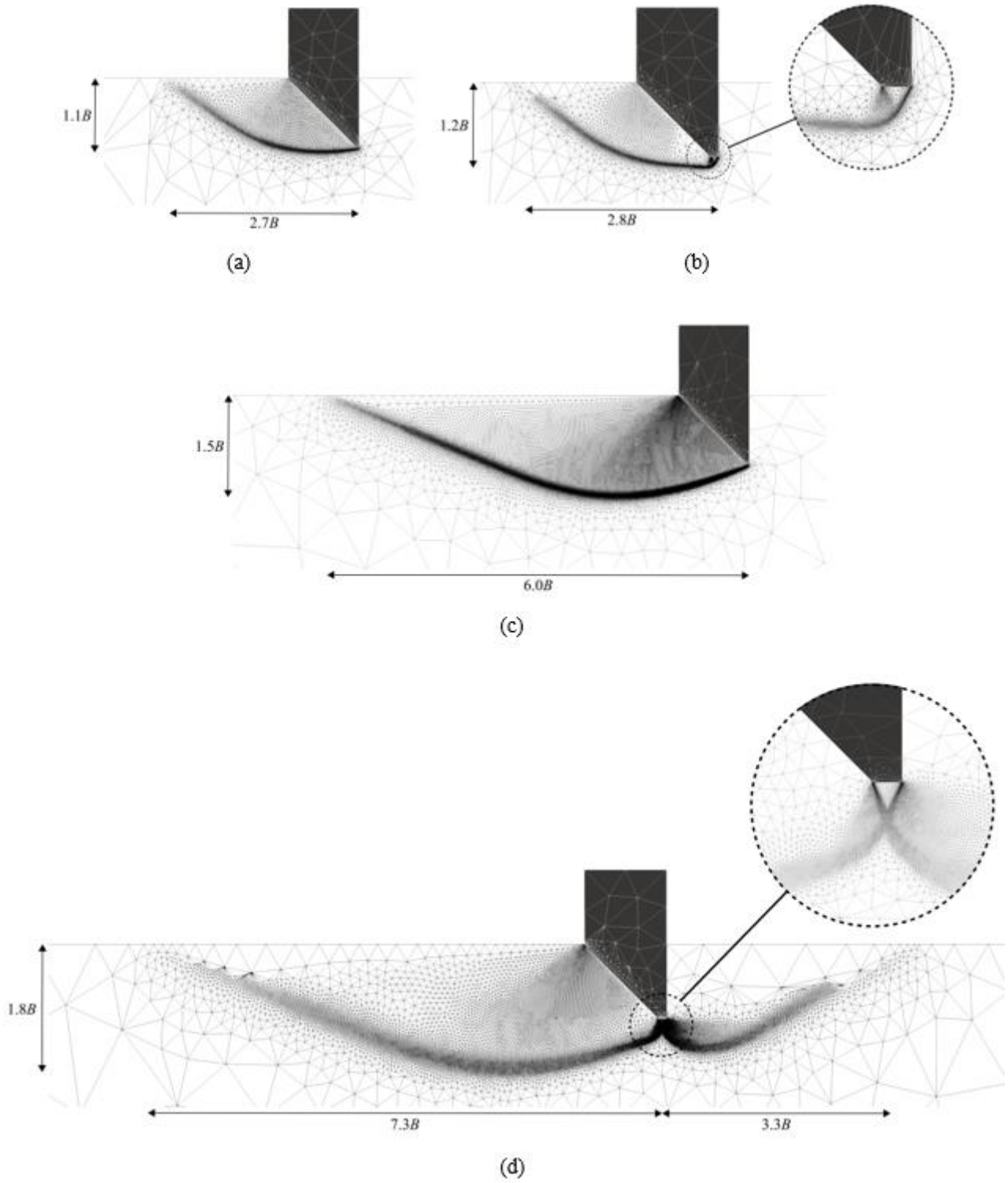


Figure 8 Numerical predictions of the soil failure mechanisms for a $\beta = 45^\circ$ footing with a smooth cutting face ($\alpha_f = 0$), using mesh refinement from the UB analysis to reveal slip line fields: (a) $t/B = 0$, $\phi' = 20^\circ$, (b) $t/B = 0.1$, $\phi' = 20^\circ$, (c) $t/B = 0$, $\phi' = 45^\circ$, and (d) $t/B = 0.1$, $\phi' = 45^\circ$; $B/R = 0$ (plane strain), $h/B = 0$, $\alpha_s = 0$, $l/B = 0$.

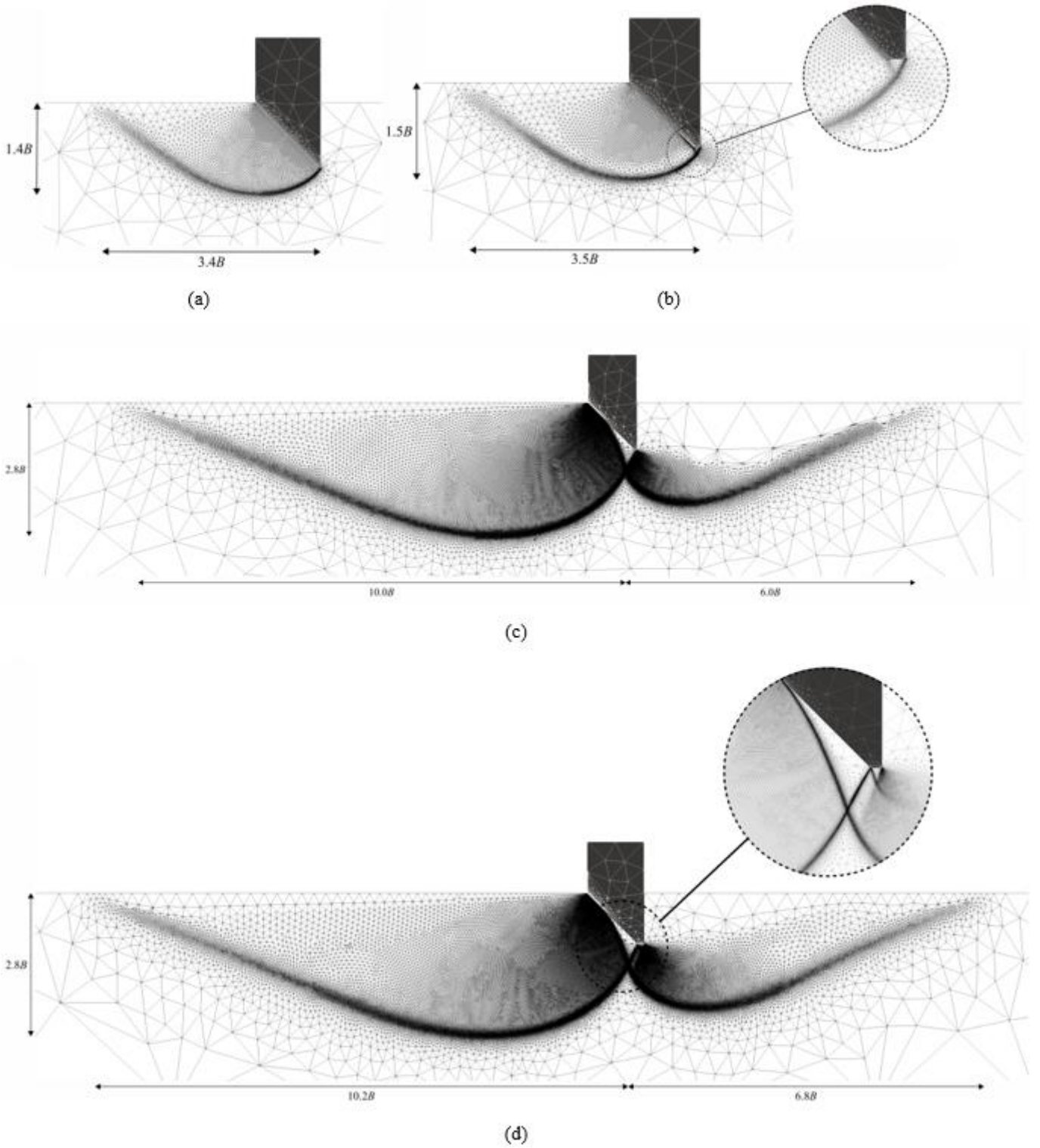
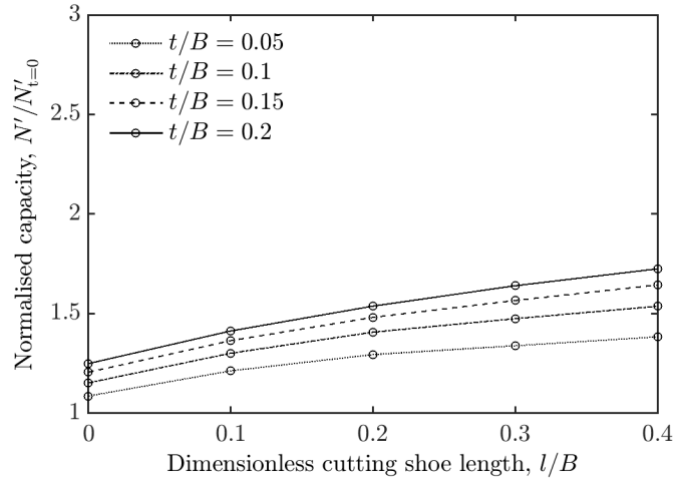
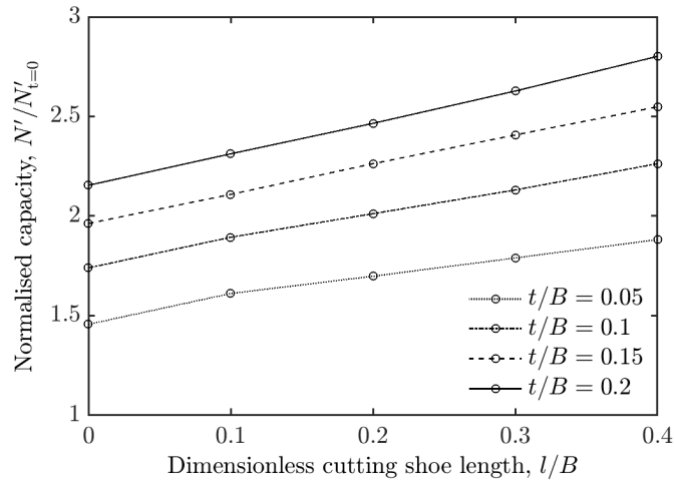


Figure 9 Numerical predictions of the soil failure mechanisms for a $\beta = 45^\circ$ footing with a rough cutting face ($\alpha_f = 1$), using mesh refinement from the UB analysis to reveal slip line fields: (a) $t/B = 0$, $\phi' = 20^\circ$, (b) $t/B = 0.1$, $\phi' = 20^\circ$, (c) $t/B = 0$, $\phi' = 45^\circ$, and (d) $t/B = 0.1$, $\phi' = 45^\circ$; $B/R = 0$ (plane strain), $h/B = 0$, $\alpha_s = 0$, $l/B = 0$.

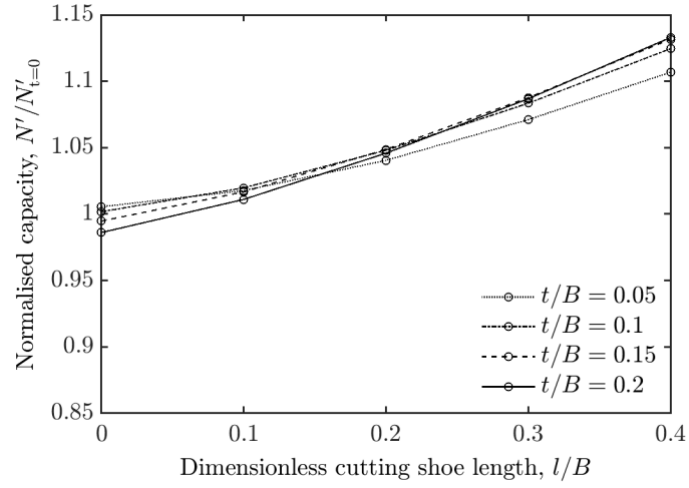


(a)

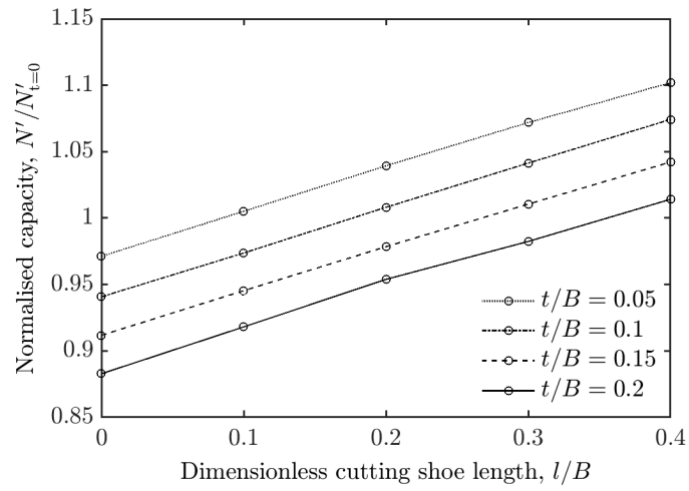


(b)

Figure 10 Numerical predictions of the influence of a cutting shoe with extension l/B on vertical bearing capacity of a $\beta = 45^\circ$ footing with a smooth cutting face ($\alpha_f = 0$): (a) $\phi' = 20^\circ$, (b) $\phi' = 45^\circ$. Results are normalised by the corresponding values for a zero cutting shoe length ($N'_{t=0}$); $B/R = 0$ (plane strain), $h/B = 0$, $\alpha_s = 0$.



(a)



(b)

Figure 11 Numerical predictions of the influence of a cutting shoe with extension length l/B on vertical bearing capacity of a $\beta = 45^\circ$ footing with a rough cutting face ($\alpha_f = 1$): (a) $\phi' = 20^\circ$, (b) $\phi' = 45^\circ$. Results are normalised by the corresponding values for a zero cutting shoe length ($N'_{t=0}$); $B/R = 0$ (plane strain), $h/B = 0$, $\alpha_s = 0$.

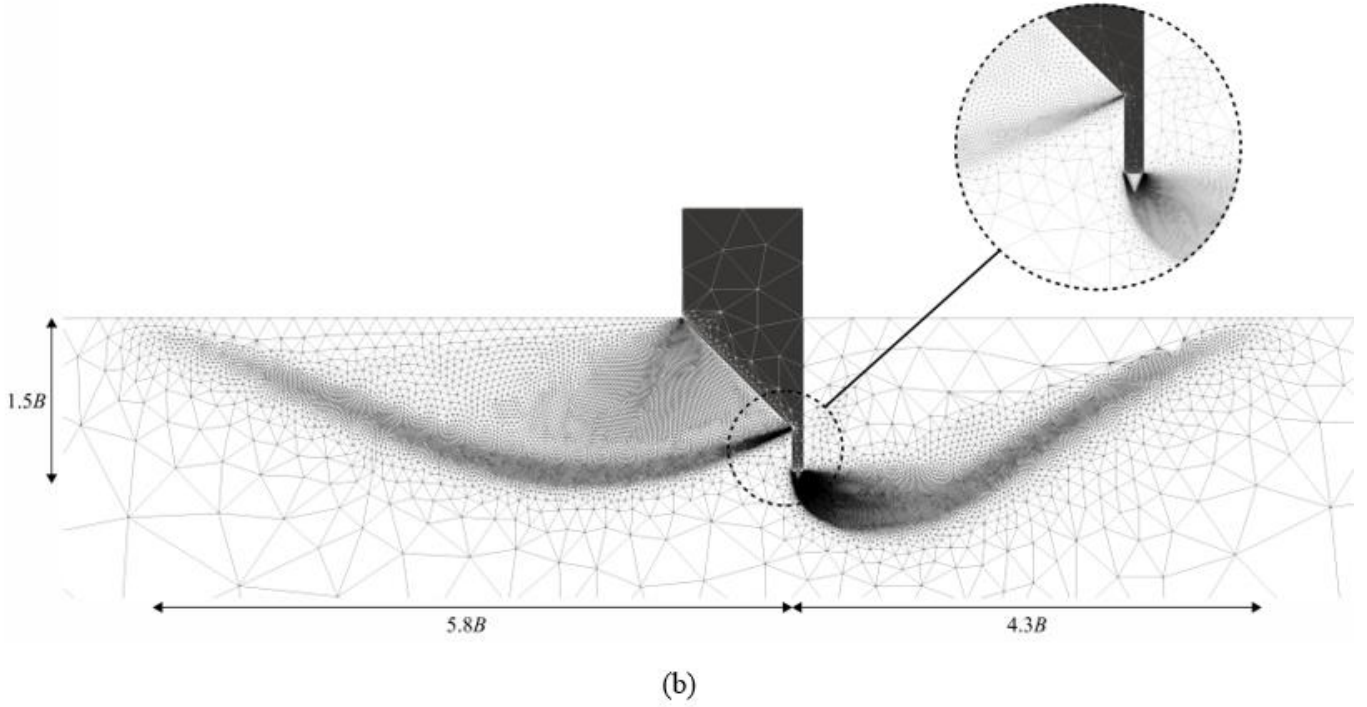
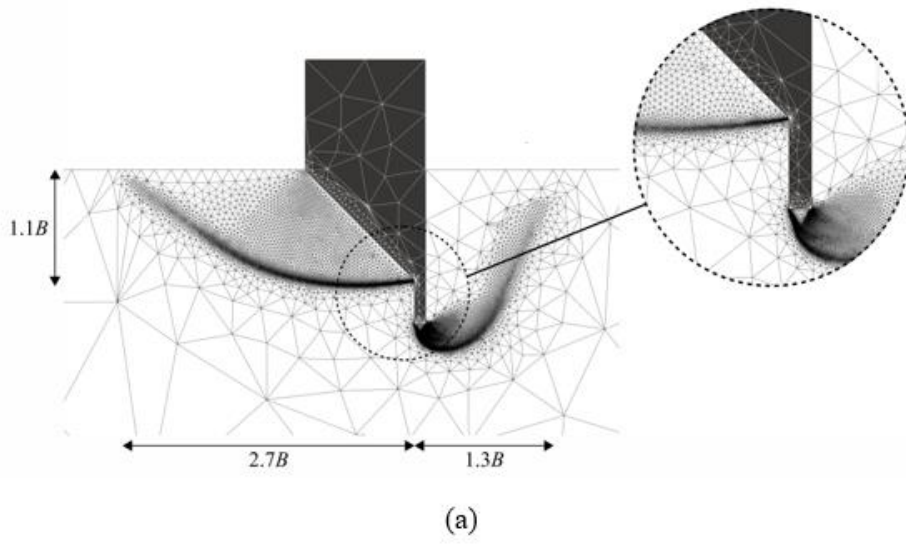


Figure 12 Numerical predictions of the soil failure mechanisms for a $\beta = 45^\circ$ footing with cutting shoe dimensions $t/B = 0.1$ and $l/B = 0.4$ and a smooth cutting face ($\alpha_f = 0$), using mesh refinement from the UB analysis to reveal slip line fields: (a) $\phi' = 20^\circ$, and (b) $\phi' = 45^\circ$; $B/R = 0$ (plane strain), $h/B = 0$, $\alpha_s = 0$.

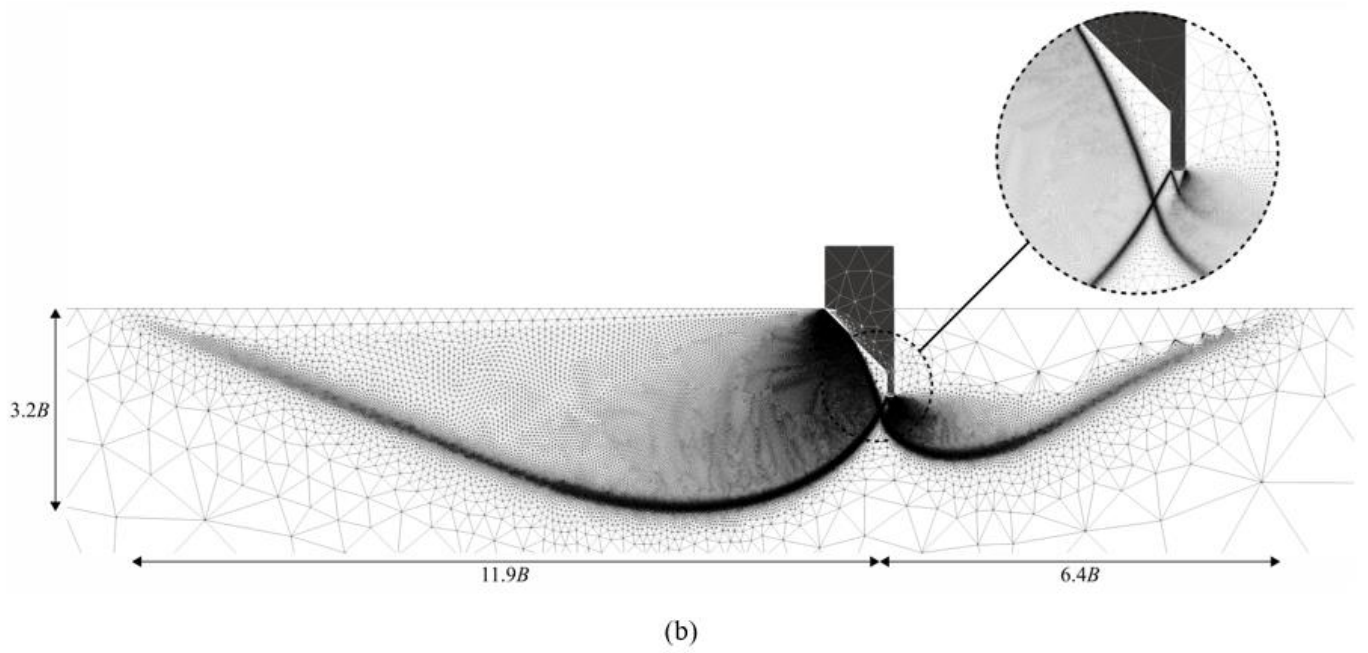
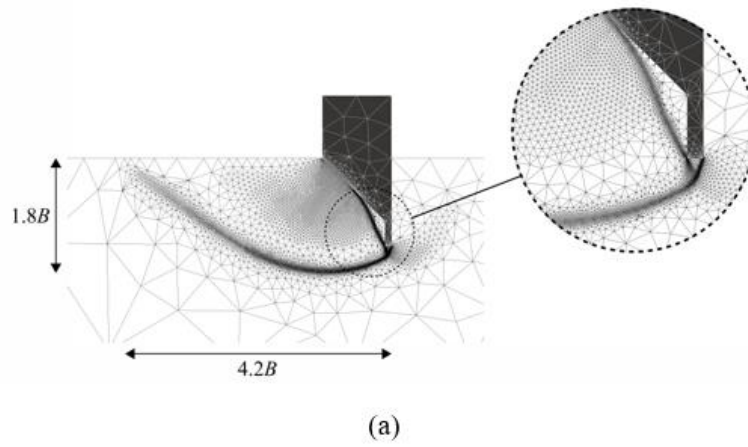


Figure 13 Numerical predictions of the soil failure mechanisms for a $\beta = 45^\circ$ footing with cutting shoe dimensions $t/B = 0.1$ and $l/B = 0.4$ and a rough cutting face ($\alpha_r = 1$), using mesh refinement from the UB analysis to reveal slip line fields: (a) $\phi' = 20^\circ$, and (b) $\phi' = 45^\circ$; $B/R = 0$ (plane strain), $h/B = 0$, $\alpha_s = 0$.

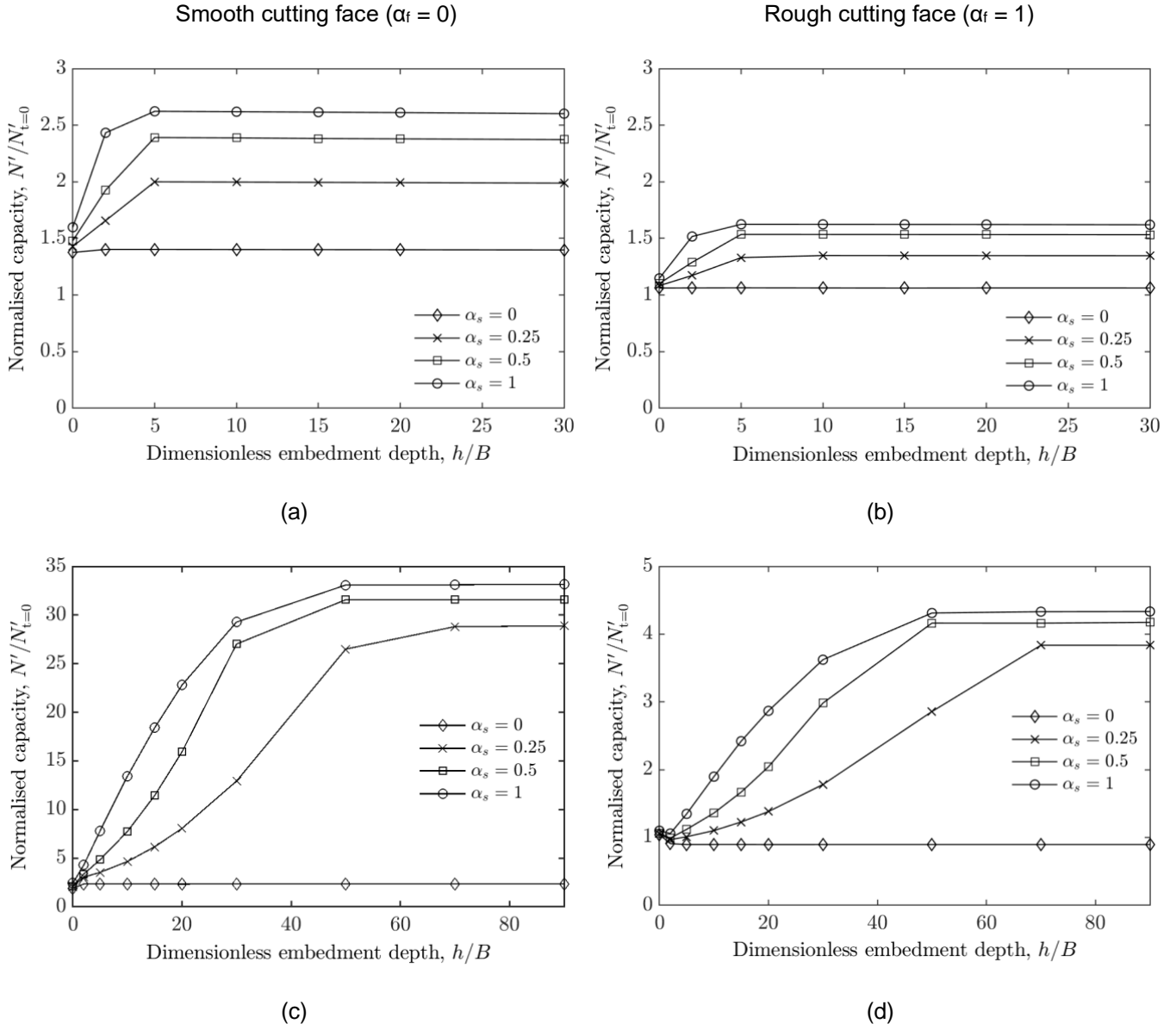


Figure 14 Numerical predictions of the influence of external embedment depth on vertical bearing capacity for a $\beta = 45^\circ$ footing with a range of cutting shoe roughness factors α_s : (a) $\alpha_f = 0$, $\phi' = 20^\circ$, (b) $\alpha_f = 1$, $\phi' = 20^\circ$, (c) $\alpha_f = 0$, $\phi' = 45^\circ$, and (d) $\alpha_f = 1$, $\phi' = 45^\circ$; $B/R = 0$ (plane strain), $t/B = 0.07$, $l/B = 0.25$ and $h_b/B = 0.25$.

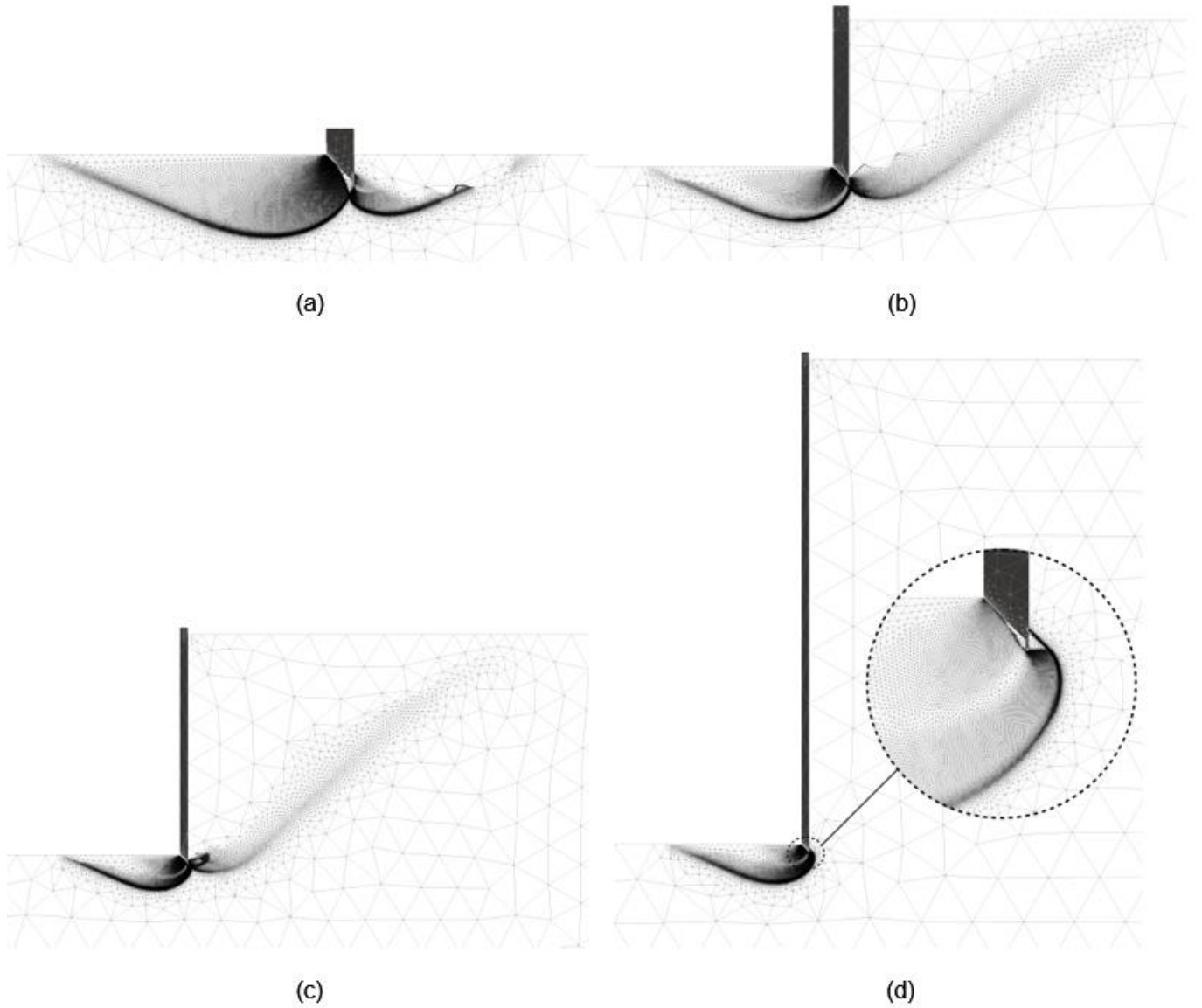
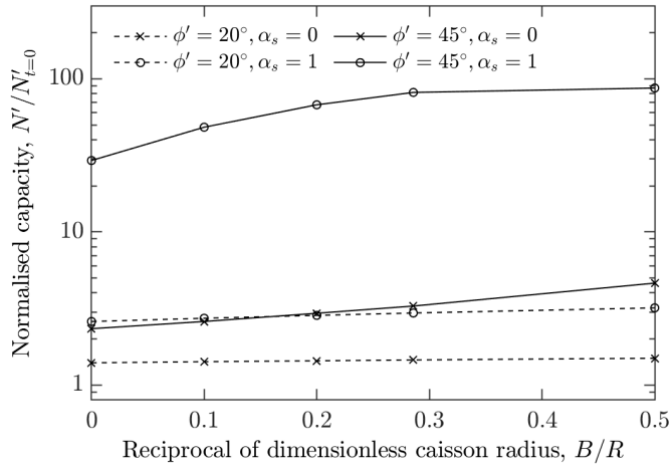
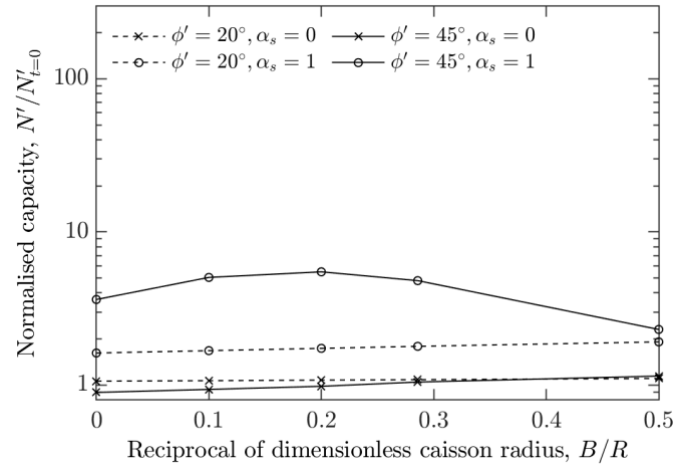


Figure 15 Numerical predictions of the soil failure mechanisms for a $\beta = 45^\circ$ footing in $\phi' = 45^\circ$ soil, using the refined mesh from an UB analysis to reveal slip line fields: (a) $h/B = 0$, (b) $h/B = 10$, (c) $h/B = 30$, (d) $h/B = 70$; $B/R = 0$ (plane strain), $\alpha_f = 1$, $\alpha_s = 1$, $t/B = 0.07$, $l/B = l_b/B = 0.25$. The models are not shown with the same scale, for clarity.



(a)



(b)

Figure 16 Numerical predictions of the influence of the reciprocal of dimensionless caisson radius B/R on vertical bearing capacity for a $\beta = 45^\circ$ footing with a range of cutting shoe roughness factor α_s : (a) $\alpha_f = 0$, and (b) $\alpha_f = 1$; $h/B = 30$, $t/B = 0.07$, $l/B = 0.25$ and $b/B = 0.25$.

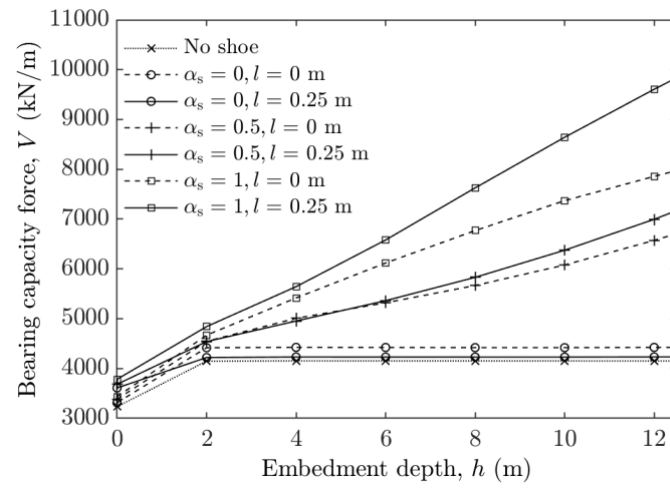


Figure 17 Numerical predictions of the vertical bearing capacity for the Blackpool case study considering various cutting shoe designs.